Noisy saltatory spike propagation: The breakdown of signal transmission due to channel noise

Y. Li[1,a], G. Schmid[1,b], and P. Hänggi[1]

Institut für Physik, Universität Augsburg, Universitätsstr. 1, 86159 Augsburg, Germany

Abstract. Noisy saltatory spike propagation along myelinated axons is studied within a stochastic Hodgkin-Huxley model. The *intrinsic* noise (whose strength is inversely proportional to the nodal membrane size) arising from fluctuations of the number of open ion channels influences the dynamics of the membrane potential in a node of Ranvier where the sodium ion channels are predominantly localized. The nodes of Ranvier are linearly coupled. As a measure for the signal propagation reliability, we focus on the ratio between the number of initiated spikes and the transmitted spikes. This work supplements our earlier study [A. Ochab-Marcinek, G. Schmid, I. Goychuk and P. Hänggi, Phys. Rev E **79**, 011904 (2009)] towards stronger channel noise intensity and supra-threshold coupling. For strong supra-threshold coupling the transmission reliability decreases with increasing channel noise level until the causal relationship is completely lost and a breakdown of the spike propagation due to the intrinsic noise is observed.

1 Introduction

As the fast propagation of action potentials along the axon is of fundamental importance in the nervous system, e.g. for the successful evolution to large body sizes of organisms, or the information processing in the brain, the study of the propagation mechanisms is of great interest for neuroscientists, physiologists and physicists [1]. Since the empirical modeling proposed by Hodgkin and Huxley in 1952 [2], the neuronal firing dynamics with respect to spike generation and signal propagation are successfully studied within this deterministic model. In recent years, issues related to the constructive role of noise in stochastic variants of these models were addressed [3,4]. The noise-assisted enhancement in weak signals transmission, transduction, or detection has been investigated, e.g. in the context of noise supported wave propagation in sub-excitable media [5] or in excitable systems [4]. The conductance fluctuation of the neuronal membranes which arises from random channel opening and closing can, *a priori* not be neglected [6,7]. Indeed, it was shown, that this intrinsic *channel noise* [3] can lead to generation of so-called *spontaneous action potentials*, to synchronization phenomena like *stochastic resonance* [8–12] and *coherence resonance* [13,14] and to synchronization of ion channel clusters [15,16].

Even the saltatory spike propagation, which results from a highly non-uniform distribution of the ion channel, can benefit from intrinsic channel noise as we have shown recently in Ref. [17]. The saltatory spike propagation occurs in myelinated axons where the activating sodium ion channels are concentrated at the nodes of Ranvier, which are separated by segments sheathed

[a] e-mail: yunyun.li@physik.uni-augsburg.de
[b] e-mail: gerhard.schmid@physik.uni-augsburg.de

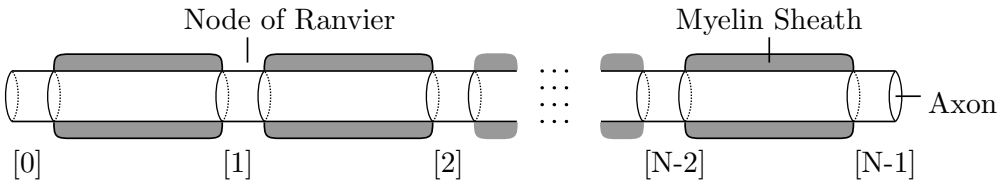

Fig. 1. Sketch of the myelinated axon: Each node of Ranvier is treated within a stochastic generalization of the Hodgkin-Huxley model and is bi-linearly coupled to the nearest neighboring nodes of Ranvier.

with myelin. This results in a much faster propagation speed in myelinated axons than that in unmyelinated axons with constant ion channel density [18,19].

With this work, we extend our prior study [17] on the effect of channel noise on the propagation of action potentials along myelinated axons. In terms of transmission reliability we discuss the influence of the coupling strength between neighboring nodes of Ranvier and that of strong intrinsic noise.

2 Model

In order to model the signal transmission along myelinated axons, we consider a compartmental stochastic Hodgkin-Huxley model [17]. Accordingly, each node of Ranvier is modeled by a stochastic generalization of the Hodgkin-Huxley model, which extends the applicability of the original Hodgkin-Huxley model [2] towards stochastic dynamics of the membrane potential of finite-size ion channel clusters [3,20]. Each node of Ranvier couples linearly to its nearest neighbors. Consequently, the membrane dynamics V_i at the ith node of Ranvier reads (with $i = 0, 1, 2, \ldots, N-1$, where N corresponds to the total number of axonal nodes of Ranvier):

$$C \frac{\mathrm{d}}{\mathrm{d}t} V_i = I_{i,\mathrm{ionic}}(V_i) + I_{i,\mathrm{inter}}(t) + I_{i,\mathrm{ext}}(t)\,, \quad \text{for } i = 0, 1, 2, ..., N-1\,, \tag{1a}$$

with the ionic membrane current (per unit area) within the ith node of Ranvier given by the Hodgkin-Huxley model [2]

$$I_{i,\mathrm{ionic}}(V_i) = -G_\mathrm{K}(n_i)\,(V_i - E_\mathrm{K}) - G_\mathrm{Na}(m_i, h_i)\,(V_i - E_\mathrm{Na}) - G_\mathrm{L}(V_i - E_\mathrm{L})\,, \tag{1b}$$

the inter-nodal currents

$$I_{i,\mathrm{inter}}(t) = \begin{cases} \kappa\,(V_{i+1} - V_i) & \text{for } i = 0\,, \\ \kappa\,(V_{i-1} - V_i) & \text{for } i = N-1\,, \\ \kappa\,(V_{i-1} - 2V_i + V_{i+1}) & \text{elsewhere} \end{cases} \tag{1c}$$

and the external current stimuli $I_{i,\mathrm{ext}}(t)$ at the ith node of Ranvier. In Eq. (1a), C denotes the capacity of the axonal membrane per unit area and is given by $C = 1\,\mu\mathrm{F/cm}^2$. The coupling strength between neighboring nodes is characterized by κ, cf. Eq. (1c). According to the Hodgkin-Huxley model [2], reversal potentials for the sodium, potassium, and leak current are $E_\mathrm{Na} = 50\,\mathrm{mV}$, $E_\mathrm{K} = -77\,\mathrm{mV}$, and $E_L = -54.4\,\mathrm{mV}$, respectively. The conductances per unit area are given by:

$$G_\mathrm{K}(n_i) = g_\mathrm{K}^\mathrm{max}\; n_i^4, \quad G_\mathrm{Na}(m_i, h_i) = g_\mathrm{Na}^\mathrm{max}\; m_i^3 h_i \tag{2}$$

and the constant leakage conductance $G_\mathrm{L} = 0.3\,\mathrm{mS/cm}^2$. In Eq. (2), $g_\mathrm{K}^\mathrm{max}$ and $g_\mathrm{Na}^\mathrm{max}$ denote the maximum potassium and sodium conductances per unit area, when all ion channels within the corresponding node are open. For simplicity, we assume that every axonal node has the same kinetics, i.e. the same number of sodium and potassium ion channels. So, the maximum potassium and sodium conductances $g_\mathrm{K}^\mathrm{max} = 36\,\mathrm{mS/cm}^2$ and $g_\mathrm{Na}^\mathrm{max} = 120\,\mathrm{mS/cm}^2$ are identical constants for every node of Ranvier.

The gating variables n_i, m_i and h_i in Eqs. (1b) and (2), describe the open probabilities of the ion channel gates in the ith node, and undergo a stochastic process which stems from a birth-and-death-like process of the gating dynamics. The dynamics of the gating variables are voltage dependent, and are governed by the set of (Ito)-stochastic differential equations [20–22],

$$\frac{\mathrm{d}}{\mathrm{d}t} x_i = \alpha_x(V_i)\ (1 - x_i) - \beta_x(V_i)\ x_i + \xi_{i,x}(t)\,, \tag{3}$$

with $x = m, h, n$. Here, $\xi_{i,x}(t)$ are Gaussian white noise with vanishing mean and vanishing cross-correlations. For the same node with the nodal membrane size $\mathcal{A}$, the non-vanishing noise correlations take the following form:

$$\langle \xi_{i,m}(t)\, \xi_{i,m}(t') \rangle = \frac{1}{\mathcal{A}\rho_{\mathrm{Na}}}\ [\alpha_m(V_i)\,(1 - m_i) + \beta_m(V_i)\, m_i]\ \delta(t - t')\,, \tag{4a}$$

$$\langle \xi_{i,h}(t)\, \xi_{i,h}(t') \rangle = \frac{1}{\mathcal{A}\rho_{\mathrm{Na}}}\ [\alpha_h(V_i)\,(1 - h_i) + \beta_h(V_i)\, h_i]\ \delta(t - t')\,, \tag{4b}$$

$$\langle \xi_{i,n}(t)\, \xi_{i,n}(t') \rangle = \frac{1}{\mathcal{A}\rho_{\mathrm{K}}}\ [\alpha_n(V_i)\,(1 - n_i) + \beta_n(V_i)\, n_i]\ \delta(t - t')\,, \tag{4c}$$

where the ion channel densities are $\rho_{\mathrm{Na}} = 60\,\mu\mathrm{m}^{-2}$ and $\rho_{\mathrm{K}} = 18\,\mu\mathrm{m}^{-2}$. The noise strength is determined by the nodal membrane size $\mathcal{A}$ which is the same for all nodes. In Eq. (3), the dynamics of the opening and closing rates $\alpha_x(V)$ and $\beta_x(V)$ ($x = m, h, n$) are taken at $T = 6.3\,^{\circ}\mathrm{C}$. They depend on the local membrane potential V and read (with numbers given in units of [mV]) [2,23]:

$$\alpha_m(V) = \frac{0.1(V + 40)}{1 - \exp\{-(V + 40)/10\}}, \tag{5a}$$

$$\beta_m(V) = 4\ \exp\{-(V + 65)/18\}\,, \tag{5b}$$

$$\alpha_h(V) = 0.07\ \exp\{-(V + 65)/20\}\,, \tag{5c}$$

$$\beta_h(V) = \frac{1}{1 + \exp\{-(V + 35)/10\}}, \tag{5d}$$

$$\alpha_n(V) = \frac{0.01(V + 55)}{1 - \exp\{-(V + 55)/10\}}, \tag{5e}$$

$$\beta_n(V) = 0.125\ \exp\{-(V + 65)/80\}\,. \tag{5f}$$

3 Spike transmission

In order to analyze the transmission reliability, we exemplary consider a chain consisting of ten nodes of Ranvier, i.e. $N = 10$ and numerically simulated Eq. (1). By applying a constant current stimulus on the first node only, i.e. we set $I_{0,\mathrm{ext}} = 12\,\mu\mathrm{A/cm}^2$ and $I_{i,\mathrm{ext}} = 0$ for $i = 1, ..., N - 1$, we find that action potentials are periodically produced that propagate along the transmission line. We define the transmission reliability coefficient $\mathcal{R}$ in steady state by the ratio of the number of action potentials arriving at the terminal node $\mathcal{N}_9$ to those generated in the initial node $\mathcal{N}_0$:

$$\text{transmission reliability coefficient: } \mathcal{R} = \frac{\mathcal{N}_9}{\mathcal{N}_0}. \tag{6}$$

The occurrence of a spike in the membrane potential $V_i(t)$ is identified by an upward-crossing of the detection barrier at 0.0 mV (further details on the numerics can be found in Ref. [17]). The spike instances t_i^j with $j = 1, ..., \mathcal{N}_i$ define point processes $u_i(t) = \sum_{j=1}^{\mathcal{N}_i} \delta(t - t_i^j)$. Here, $\mathcal{N}_i$ indicates the number of spikes on the ith node.

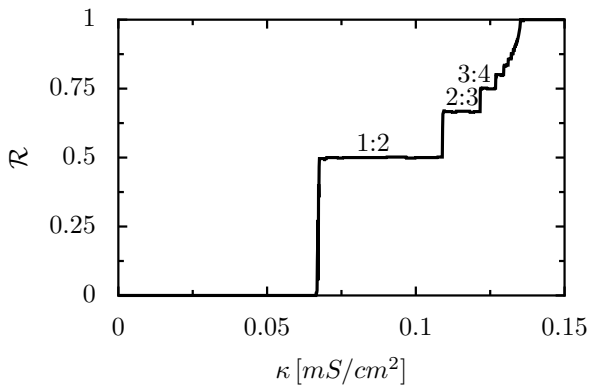

Fig. 2. Deterministic transmission reliability: The dependence of the transmission reliability $\mathcal{R}$ on the inter-nodal coupling strength κ is depicted for the deterministic case. For sub-threshold $\kappa \lesssim 0.067\,\mathrm{mS/cm^2}$, no spike propagation is observed, i.e. $\mathcal{R} = 0$. Perfect spike transmission, i.e. $\mathcal{R} = 1$, is found for the supra-threshold case $\kappa \gtrsim 0.136\,\mathrm{mS/cm^2}$. In the intermediate range rational numbers $k : l$ for the transmission reliability are found.

3.1 Deterministic dynamics

We start with the deterministic limit which is formally achieved in the limit $\mathcal{A} \to \infty$, using $N = 10$. In this case, the transmission reliability $\mathcal{R}$ depends solely on the inter-nodal coupling strength κ and exhibits distinguished transmission patterns [17].

The dependence of the transmission reliability $\mathcal{R}$ on the coupling strength is depicted in Fig. 2. For sub-threshold coupling, i.e. $\kappa \lesssim 0.067\,\mathrm{mS/cm^2}$ the ratio equals zero and no spike propagation to the final node is observed. Contrary, for sufficiently large coupling parameter, i.e. $\kappa \gtrsim 0.136\,\mathrm{mS/cm^2}$, each generated action potential propagates along the axon and arrives at the final node, i.e. $\mathcal{R} = 1$. Discrete, rational transmission patterns $k : l$ appear for intermediate values of the coupling parameter.

3.2 Channel noise effects

When considering finite sizes $\mathcal{A}$ of the nodes of Ranvier, the staircase-like dependence of the transmission reliability parameter $\mathcal{R}$, which is depicted in Fig. 2 for the deterministic case (i.e. for the case of an infinite size of the nodes of Ranvier), turns into a continuous dependence (not shown).

In the limit of strong intrinsic noise, i.e. for the finite size of the nodes of Ranvier approaching formally zero, the channel noise reigns the dynamics of the membrane potential of each node and the influence of the bi-linear coupling becomes negligible. Consequently, in this limit the causal relationship between spiking in the first node and that one in the terminal node is lost. The number of spike occurrences at the final node does not markedly depend on the actual value of the coupling parameter, and the ratio $\mathcal{R}$ tends to a value independent of coupling strength κ, cf. Fig. 3. Note that in this case, the information transfer from an initial to a final node fades towards zero as the correlation between spikes in the initial and the final node diminishes. Moreover, the spontaneous spikes stimulate via the coupling the neighboring nodes and, consequently, a transmission to both sides occurs, cf. Fig. 4 (c). In the limit $\kappa \to 0$, the initial and the terminal node are spiking independently. Consequently, $\mathcal{R}$ is given by the ratio of the number of spontaneous spikes occurring within the non-stimulated, stochastic Hodgkin-Huxley dynamics and the number of spikes occurring within the stochastic Hodgkin-Huxley dynamics complemented by a constant current stimulus of $I = 12\,\mu\mathrm{A/cm^2}$. Certainly, the causal relationship is lost in this case. This becomes evident when considering the cross-correlation between the spiking of the initial and that of the final node (see below).

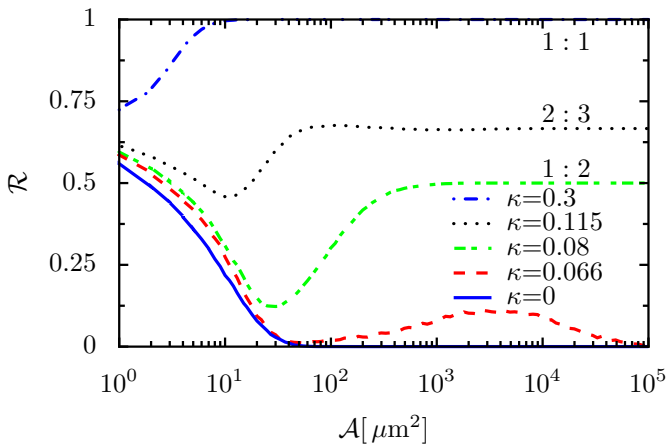

Fig. 3. (Color online) Transmission reliability in presence of channel noise: The transmission reliability coefficient $\mathcal{R}$ is plotted against the membrane size of the node of Ranvier for different strengths of the inter-nodal coupling (the coupling strengths are given in units of mS/cm^2). The data confirm the results for noise-assisted spike propagation for sub-threshold coupling (see dashed red line) [17]. Moreover, the minimum in $\mathcal{R}$ indicates the cross-over from a stochastic, uncorrelated spiking of the initial and final nodes towards a causal, noisy spike transmission from the initial to the final node.

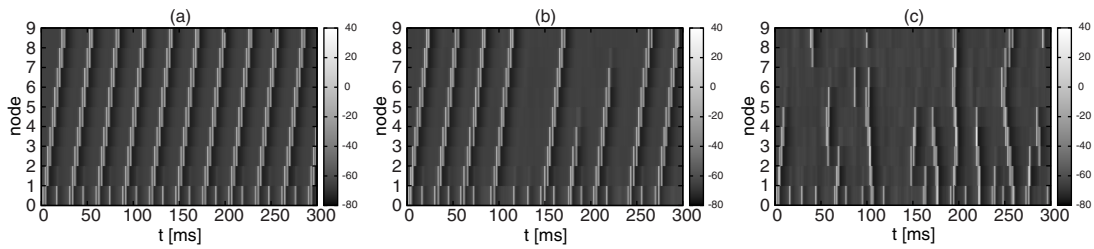

Fig. 4. Spatio-temporal transmission patterns of spike propagation: the spatio-temporal evolution of the membrane dynamics at different axonal nodes of Ranvier is plotted for an intermediate coupling strength $\kappa = 0.08\,mS/cm^2$ and various nodal membrane sizes: (a) $\mathcal{A} = 3 \cdot 10^4\,\mu m^2$ (low channel noise level); (b) $\mathcal{A} = 100\,\mu m^2$ (intermediate channel noise level) and (c) $\mathcal{A} = 10\,\mu m^2$ (high channel noise level). Next to each panel, there is a grayscale bar indicating the actual value of the membrane potential. The action potentials are created by a current stimulus at the initial node ("0"). In the case of low noise level, cf. panel (a), the deterministic transmission pattern of 2 : 1 is clearly visible. In contrast, in the strong noise limit, due to the dominating spontaneous spiking, irregular transmission is found.

With increasing size of the nodes of the Ranvier $\mathcal{A}$, i.e. with decreasing channel noise strength, the transmission becomes more regular, cf. Fig. 4(a) and (b). The causal relationship is restored in this limit and the transmission coefficient $\mathcal{R}$ tends to its deterministic limit. This cross-over from the stochastic non-causal firing regime to the regime of noisy spike transmission depends on the coupling strength. For smaller coupling strengths, this cross-over occurs at larger nodal membrane sizes $\mathcal{A}$, cf. Fig. 3.

Starting out from the weak noise limit, an increase in the noise strength results in a noise-assisted spike propagation phenomenon for sub-threshold coupling as pointed out before with Ref. [17]. The transmission reliability exhibits a maximum, indicating an optimal, noise assisted spike propagation, cf. Fig. 3. In this case the coupling between the nodes does not result in an efficient propagation of the spikes and the presence of intrinsic noise is necessary to overcome the threshold for excitation. However, for the supra-threshold coupling, the channel noise leads to noise-induced propagation failures and the transmission reliability coefficient $\mathcal{R}$ first decreases with increasing noise level, cf. Fig. 3. The observed increase of $\mathcal{R}$ for strong intrinsic

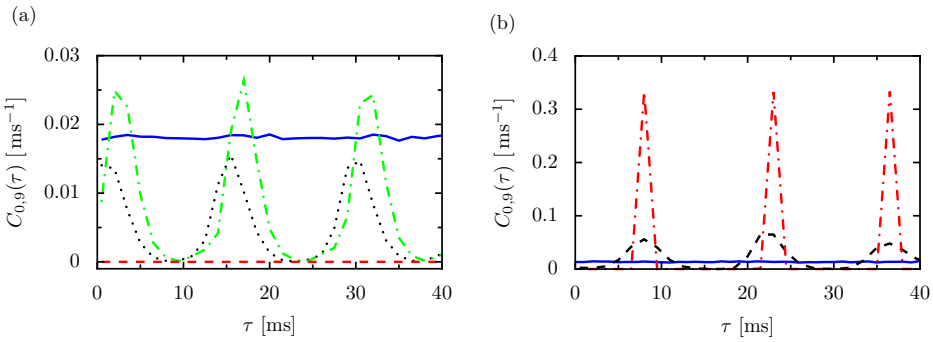

Fig. 5. (Color online) Initial-final-node spiking correlation: The spike correlation $C_{0,9}(\tau)$ between the spiking at the initial node and that of the final node, cf. Eq. (9), is plotted for different coupling strengths κ and membrane sizes $\mathcal{A}$: In panel (a), for sub-threshold coupling $\kappa = 0.066\,\mathrm{mS/cm^2}$ and membrane sizes $\mathcal{A} = 10\,\mu\mathrm{m}^2$ (blue solid line), $\mathcal{A} = 800\,\mu\mathrm{m}^2$ (black dotted line), $\mathcal{A} = 3 \cdot 10^3\,\mu\mathrm{m}^2$ (green dash-dotted line), and $\mathcal{A} = 5 \cdot 10^5\,\mu\mathrm{m}^2$ (red dashed line); In panel (b), for supra-threshold coupling $\kappa = 0.08\,\mathrm{mS/cm^2}$ and membrane sizes $\mathcal{A} = 10\,\mu\mathrm{m}^2$ (blue solid line), $\mathcal{A} = 100\,\mu\mathrm{m}^2$ (black dashed line), $\mathcal{A} = 3 \cdot 10^4\,\mu\mathrm{m}^2$ (red dash-dotted line). For weak intrinsic noise, the sharp peak indicates a strong correlation. In contrast, in the strong noise limit the causal relationship is lost and the correlation function does not exhibit a peak. Interestingly, for the sub-threshold case a shift of the peak towards shorter times is observed, i.e. there is a speed up of the signal transmission with increasing noise level.

noise is attributed to the cross-over to the stochastic, non-causal firing regime accompanied by uncorrelated spiking in the initial and final nodes.

In order to analyze the spike correlation between the initial and final node, we first segment the point processes $u_0(t)$ and $u_9(t+\tau)$ in segments of width Δt. For Δt smaller than the refractory time, there is either no spike or one spike observable in each segment. For our analysis, we chose $\Delta t = 1.5\,\mathrm{ms}$. In a second step, we determine the number of spike coincidences $\mathcal{N}_{0,9}(\tau)$ between the initial node and the final node in the segments of width Δt, i.e. the spike coincidences between the two point processes $u_0(t)$ and $u_9(t+\tau)$:

$$\mathcal{N}_{0,9}(\tau) = \Delta t \int_0^T \mathrm{d}t\, f_0(t) f_9(t+\tau)\,, \tag{7}$$

where the point process $u_i(t)$ is approximated by

$$f_i(t) = \int_t^{t+\Delta t} \mathrm{d}t' u_i(t')/\Delta t \;\text{ for } i = 0, 9\,. \tag{8}$$

In Eq. (7), T denotes the total integration time. Note that the above definition corresponds to a cross-correlation measure. Thirdly, we relate this number $\mathcal{N}_{0,9}(\tau)$ to the number of initiated spikes at node "0", i.e. $\mathcal{N}_0$, and the bin-width Δt. We obtain the probability density $C_{0,9}(\tau)$:

$$C_{0,9}(\tau) = \frac{\mathcal{N}_{0,9}(\tau)}{\Delta t\, \mathcal{N}_0} = \frac{1}{\mathcal{N}_0} \int_0^T \mathrm{d}t\, f_0(t) f_9(t+\tau)\,. \tag{9}$$

Note that due to the periodic spike initiation at the first node, $C_{0,9}(\tau)$ is periodic, cf. Fig. 5. The normalization to the total number of initiated spikes $\mathcal{N}_0$ ensures that the integral of $C_{0,9}(\tau)$ over one period results in the transmission coefficient $\mathcal{R}$ defined by Eq. (6).

A sharp peak in $C_{0,9}(\tau)$ indicates a high correlation. For supra-threshold coupling and weak intrinsic noise, the correlation measure $C_{0,9}(\tau)$ exhibits a sharp peak for a τ-value, which corresponds to the propagation time modulo the period of the spiking in the initial node, cf. Fig. 5(b). With increasing noise level, the width of the peak increases and the height of the peak compared to the background level decreases until the total disappearance of the peak in the

background showing the lost of any causal correlation. Interestingly, for the sub-threshold case, not only a broadening and flattening of the peak can be observed with increasing noise level, but also a shift of the peak towards smaller τ-values showing a speed up of the transmission, cf. Fig. 5(a). The latter can be explained by the same line of reasoning as was used in the discussion of *anticipated synchronization* in Ref. [24].

4 Conclusion

We numerically studied the saltatory spike propagation along a myelinated axon using a multi-compartmental stochastic Hodgkin-Huxley model. The channel noise affecting the dynamics of the bi-linearly coupled nodes of Ranvier originates in the random ion channel gating. For the spike propagation in terms of transmission reliability (ratio of the number of spike observed in the terminal node to the number of spikes initiated in the first node), we found a reduction of reliability with increasing channel noise level for supra-threshold coupling. This is due to the noise-induced propagation failures. A further increase of the channel noise level leads to the total loss of the spiking correlation between the first and last node of Ranvier in the axonal chain. In the case of sub-threshold coupling and moderate channel noise level, the channel noise can constructively contribute to the spike propagation, and the effect of noise-assisted spike propagation is recovered. Both, the transmission reliability as well as the propagation speed can increase with increasing channel noise level. This behavior is quite similar to the phenomenon of stochastic resonance [8–10] with an intrinsic noise source [11,12] with the internodal coupling playing the role of a nodal stimulus.

The authors like to applaud and warmly thank Lutz Schimansky-Geier for his continuous engagement in furthering stochastic physics within the statistical physics community worldwide and for his many elucidative discussions with us in pursuing stochastic physics. He is still young and strong enough to appreciate and to contribute great science.

References

1. B.B. Averbeck, D. Lee, Trends Neurosci. **27**, 225 (2004)
2. A.L. Hodgkin, A.F. Huxley, J. Physiol. **117**, 500 (1952)
3. J.A. White, J.T. Rubinstein, A.R. Kay, Trends Neurosci. **23**, 131 (2000)
4. B. Lindner, J. García-Ojalvo, A. Neiman, L. Schimansky-Geier, Phys. Rep. **392**, 321 (2004)
5. F. Sagués, J.M. Sancho, J. García-Ojalvo, Rev. Mod. Phys. **79**, 829 (2007)
6. H. Lecar, R. Nossal, Biophys. J. **11**, 1048 (1971)
7. H. Lecar, R. Nossal, Biophys. J. **11**, 1068 (1971)
8. L. Gammaitoni, P. Hänggi, P. Jung, F. Marchesoni, Rev. Mod. Phys. **70**, 223 (1998)
9. V.S. Anishchenko, A.B. Neiman, F. Moss, L. Shimansky-Geier, Usp. Fiz. Nauk. **169**, 7 (1999)
10. P. Hänggi, Chem. Phys. Chem. **3**, 285 (2002)
11. G. Schmid, I. Goychuk, P. Hänggi, Europhys. Lett. **56**, 22 (2001)
12. P. Jung, J.W. Shuai, Europhys. Lett. **56**, 29 (2001)
13. G. Schmid, I. Goychuk, P. Hänggi, Phys. Biol. **1**, 61 (2004)
14. G. Schmid, I. Goychuk, P. Hänggi, Phys. Biol. **3**, 248 (2006)
15. S. Zeng, Y. Tang, P. Jung, Phys. Rev. E **76**, 011905 (2007)
16. S. Zeng, P. Jung, Phys. Rev. E **71**, 011910 (2005)
17. A. Ochab-Marcinek, G. Schmid, I. Goychuk, P. Hänggi, Phys. Rev. E **79**, 011904 (2009)
18. C. Koch, *Biophysics of Computation, Information Processing in Single Neurons* (Oxford University Press, New York, 1999)
19. J. Keener, J. Sneyd, *Mathematical Physiology* (Springer, New York, 2001)
20. R.F. Fox, Y.N. Lu, Phys. Rev. E **49**, 3421 (1994)
21. H.C. Tuckwell, J. Theor. Biol. **127**, 427 (1987)
22. P. Hänggi, H. Thomas, Phys. Rep. **88**, 207 (1982); see Sect. 6.2
23. I. Goychuk, P. Hänggi, Proc. Natl. Acad. Sci. USA **99**, 3552 (2002)
24. G. Schmid, I. Goychuk, P. Hänggi, Physica A **325**, 165 (2003)